

# Contact Analysis and Static Load Carrying Capacity of Planetary Roller Screw Mechanism

Nam Su Kim (✉ [NS.KIM@star-co.net.kp](mailto:NS.KIM@star-co.net.kp))

Kim Il Sung University

Kyongho Kim

Kim Il Sung University

Sinhyok Jong

Kim Il Sung University

---

## Original Article

**Keywords:** Planetary roller screw, Contact analysis, Static load carrying capacity, FE model

**Posted Date:** November 17th, 2020

**DOI:** <https://doi.org/10.21203/rs.3.rs-106438/v1>

**License:** © ⓘ This work is licensed under a Creative Commons Attribution 4.0 International License.

[Read Full License](#)

---

## ORIGINAL ARTICLE

Contact Analysis and Static Load Carrying Capacity of Planetary  
Roller Screw Mechanism

Nam Su Kim\* Kyong Ho Kim and Sin Hyok Jong\*

*Faculty of Mechanics, Kim Il Sung University, Taesong District, Pyongyang, Democratic People's Republic of Korea*

---

**Abstract**

This paper aims to investigate the contact characteristics and static load carrying capacity of planetary roller screw mechanism (PRSM). Compared to the ball screw mechanism, the advantages of the PRSM are high stiffness, high load capacity, long travel life and compact structure, etc., since the PRSM possesses more contact points than ball screws in a comparable size. The actuated load is carried through the threaded surface contacts of the screw, the rollers and the nut and the contact characteristics of these components are very important for studying the wear, transmission accuracy and efficiency of a PRSM. Prior work has neglected to take a fundamental approach towards understanding the elastic-plastic contact characteristics of threaded surfaces under high loads and it is closely related to the static load carrying capacity of PRSM. Accordingly, in this paper, the contact characteristics of PRSM under the different working loads are modeled based on Hertz contact theory and the calculation formulas between normal force of thread turns and the elastic-plastic contact stress and deformation are derived. Then, it goes further to derive a calculation method of static load carrying capacity of PRSM based on simplified model of static load distribution. Finally, a verification model is developed by finite element method (FEM) to perform contact stress and strain analysis of PRSM. Besides, through the comparison of the results between the theory model and ANSYS Workbench finite element model verify the reliability of the theory.

**Key words:** Planetary roller screw, Contact analysis, Static load carrying capacity, FE model.

---

**1. Introduction**

Planetary roller screw mechanism (PRSM) is a mechanical transmission device for converting rotational motion into linear motion or vice versa.

Due to the more advanced design principles of the PRSM, it can withstand tens of thousands of hours of heavy loads in an extremely hard working environment.

In recent years the PRSM has been established as a component for applications with high frequent work schedules, high carrying capacity, and high precision, such as the medical industry, optical equipment, robotics, precision machine tools, and aerospace industry [1].

Since their invention several designs with different characteristics have been developed and patented.

Earlier work on PRSM has included research on the selection of structure parameters [2,3], kinematics and efficiency analysis [4-6], load distribution among

\* Corresponding author e-mail: [NS.KIM@star-co.net.kp](mailto:NS.KIM@star-co.net.kp).

threads [7–9], static and dynamic stiffness [10–12], transmission accuracy [13–15], lubrication and wear behaviour [16–17], manufacturing [18], dynamics [19–20], and thermal characteristics [21].

Meanwhile, in the study of contact characteristics of threaded surfaces, only a limited number of contact models of the PRSM have been proposed.

Blinov et al. [22] proposed a numerical method for determining the contact positions and axial clearance at the screw roller interface.

Jones and Velinsky [23] introduced the principle of conjugate surfaces to establish a contact kinematical model at the screw-roller and nut-roller interfaces.

Liu et al. [24] calculated the contact positions at the screw-roller and nut-roller interfaces in the PRSM, in which the helical angles of the screw, nut and rollers were identical, and derived the transmission ratio of the PRSM.

Ryakhovskiy et al. [25] calculated the contact positions and axial clearance at the roller/nut interface in an inverted PRSM by using the same method as Reference [22].

Fu et al. [26] proposed a method to calculate both the contact positions and axial clearances in an idealized PRSM design. The existing researches provide a theoretical basis for the modelling and analysis of the contact characteristics.

Besides, Auregan et al. [16–17] developed a specific apparatus to reproduce a simplified version of the contact features of a PRSM. They performed the tests in dry friction conditions, and two damage modes were identified for sufficiently low shear stresses: abrasion and fatigue.

Sandu et al. [27] provided detailed information on how the shape, size and orientation of the contact areas between threads can be obtained.

Ma et al. [28] investigated the nature of the contact with friction between the threaded surfaces in a PRSM.

From the perspective of mechanics, Abevi et al. [12] studied the static behaviour of the inverted PRSM through 3D finite element method and experiment.

The model described the static behaviour of the mechanism under a heavy load and showed the state of contacts and the stress zones in-depth.

Hojjat et al. [29] analysed the capabilities and limitations of the PRSM and proved that both large leads and extremely small leads could be easily obtained in the PRSM. The slip phenomenon was also studied regarding the forces acting on the rollers during the rotation of the screw.

Zu et al. [30] studied the structural design method and load bearing characteristics of the PRSM in accordance with the requirements of the load and efficiency of aerospace conditions.

The above references provide useful ideas for contact modelling and contact analysis, but the elastic-plastic contact characteristics of threaded surfaces under high loads are not mentioned.

Also, the reasonable calculation method of static load carrying capacity is not mentioned in former-mentioned references.

Accordingly, due to the shortcomings mentioned above, current paper investigates the elastic-plastic contact characteristics of threaded surfaces and static load carrying capacity of PRSM.

First, modelling of elastic-plastic analysis of contact characteristics among threads of the screw, roller and nut are implemented.

Then, a calculation method of static load carrying capacity of PRSM based on simplified model of static load distribution is derived.

Finally, the elastic-plastic deformation and stress of the contact ellipse of threaded surfaces are analysed in detail and the correctness of the analytical model presented in this paper is verified by FE analysis.

## 2. Modelling of contact analysis of PRSM

### 2.1. Static description of the contact characteristics

As shown in [Figure 1](#), the principal components of a standard PRSM are the screw, nut, rollers, ring gears and planetary carriers.

Screw and nut have threaded profiles with straight flanks and multi-start threads.

The rollers have single-start threads with convex flanks which reduce the friction at the interfaces [2,3].

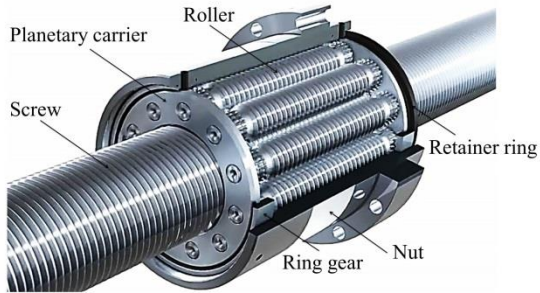


Figure 1. Structure of the PRSM.

The gear teeth mesh with the ring gear, which allows the roller to run smoothly in the axial direction. The planetary carrier is used to lock the flap.

The power and motion are transmitted through the threaded surface contacts of these components. When a load is applied to a PRSM, the stress and deformation occurs between the contact surfaces, which introduces a normal force to the contact surface. In order to consider this contact characteristics conveniently, series of equivalent balls with radius  $R$  can be used to replace rollers as the profile of rollers are rounded. [3]

And also it is assumed that the resulting contact area is an ellipse whose characteristics can be calculated using the Hertz theory. [32]

For unique loading direction, only one side of the thread works because of axial backlash.

The principal curvature parameters at contact point S between screw and roller can be written as follows (Figure 2):

$$\begin{cases} \rho_{11} = \rho_{12} = \frac{1}{R} \\ \rho_{21} = 0, \rho_{22} = \frac{2 \cos \beta}{d_c - 2R \cos \beta} \end{cases} \quad (1)$$

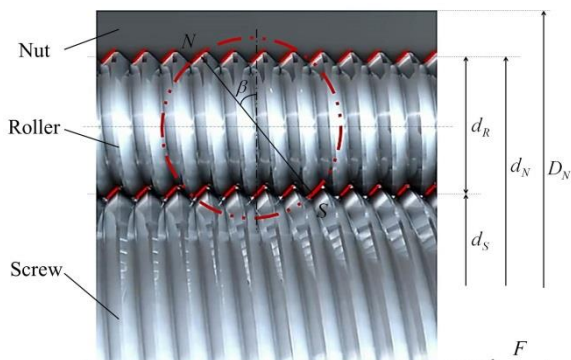


Figure 2. Equivalent ball and contact mechanism of the PRSM.

Similarly, the principal curvature parameters at contact point N between nut and roller are as follows.

$$\begin{cases} \rho_{11} = \rho_{12} = \frac{1}{R} \\ \rho_{21} = 0, \rho_{22} = -\frac{2 \cos \beta}{d_c + 2R \cos \beta} \end{cases} \quad (2)$$

where  $R$  denotes the radius of equivalent ball, as shown in Figure 2, and can be written as

$$R = \frac{d_R}{2 \cos \beta} \quad (3)$$

where  $\beta$  is the contact angle.  $F(\rho)$  is expressed as a function of curvature.

$$F(\rho) = \frac{(\rho_{11} - \rho_{12}) + (\rho_{21} - \rho_{22})}{\sum \rho} \quad (4)$$

where  $\sum \rho$  is the sum of principal curvatures of two contact objects.

In addition, the relationship between the function of curvature  $F(\rho)$  and the eccentricity of contact ellipse  $e$  can be described as follows [5]:

$$F(\rho) = \frac{(2 - e^2)L(e) - 2(1 - e^2)K(e)}{e^2 L(e)} \quad (5)$$

where  $K(e)$  is the complete elliptic integral of the first kind and  $L(e)$  is the complete elliptic integral of the second kind.

The dimensionless coefficients  $m_a$  and  $m_b$  are approximated as

$$\begin{cases} m_a = \sqrt[3]{\frac{2L(e)}{\pi k^2}} \\ m_b = \sqrt[3]{\frac{2kL(e)}{\pi}} \end{cases} \quad (6)$$

where  $k = b/a$  with  $a$  and  $b$  being the half lengths of the major and minor axis of the elliptical contact surface as

$$a = m_a \sqrt[3]{\frac{3F_n}{E' \sum \rho}} \quad (7)$$

$$b = m_b \sqrt[3]{\frac{3F_n}{E' \sum \rho}} \quad (8)$$

where  $F_n$  is the force on the normal direction of the interface.

For a specific solution of  $F(\rho)$ , the parameters  $m_a$ ,  $m_b$  and  $2k(e)/\pi m_a$  can be obtained from the relevant table given in [3].

$E'$  is the equivalent Young's modulus, which can be explicitly shown as

$$\frac{2}{E'} = \frac{(1-\mu_1^2)}{E_1} + \frac{(1-\mu_2^2)}{E_2} \quad (9)$$

where  $E_1$  and  $E_2$  are the elastic modulus and  $\mu_1$  and  $\mu_2$  are the Poisson's ratio of two contact objects.

### 2.2. Contact stress

When the axial static load is applied to a PRSM, the contact stress and the elastic deformation occurs between the contact surfaces, which introduces a normal force to the contact surface at first.

If the equivalent stress in the contact area has reached the yield stress of the material of a PRSM, the plastic deformation begins to occur as the external load increases.

In general, the stress-strain relationship of the elastoplastic material follows in the idealized elastic-plastic model or the linear strain-hardening elastic-plastic model.

Above them, the latter is more reasonable for the material of the main components of a PRSM than the former.

The stress-strain relationship according to the linear strain-hardening elastic-plastic model can be written as

$$\sigma = \begin{cases} E'\varepsilon & (|\varepsilon| \leq |\varepsilon_S|) \\ \sigma_S + E'_p(\varepsilon - \varepsilon_S) & (\varepsilon > \varepsilon_S) \\ -\sigma_S - E'_p(\varepsilon - \varepsilon_S) & (\varepsilon < -\varepsilon_S) \end{cases} \quad (10)$$

As shown in Figure 3, the stress distribution over the ellipse contact area is semi-elliptical sphere due to hertz theory of elastic contact. [32]

The contact stress distribution of threaded surfaces can be written as

$$\sigma(x, y) = \sigma_{\max} \sqrt{1 - \frac{x^2}{a^2} - \frac{y^2}{b^2}} \quad (11)$$

The total normal force  $F_n$  on the contact area under pressure is equal to

$$F_n = \int \sigma(x, y) ds = \frac{2}{3} \pi ab \sigma_{\max} \quad (12)$$

The maximum pressure  $\sigma_{\max}$  in the center of the contact area can be calculated as a function of the total normal force  $F_n$ .

$$\sigma_{\max} = \frac{3F_n}{2\pi ab} \quad (13)$$

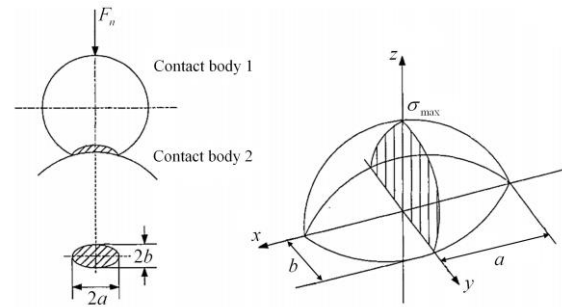


Figure 3. Elastic contact stress over the ellipse contact area.

In order to model the perfect plastic behaviour of the contact stress corresponding to the linear strain-hardening elastic-plastic characteristics of the contacting materials, we make some simplified assumptions in this paper as follows:

**Assumption 1.** During the plastic loading, the total contact stress of the threaded surface is sum of the elastic limit stress and the additional contact stress due to the hardening effect.

$$\sigma = \sigma_{EL} + \sigma_P \quad (14)$$

**Assumption 2.** The additional contact stress distribution is also semi-elliptical sphere due to hertz theory of elastic contact. (Figure 4)

$$\sigma_P(x, y) = \sigma_{\max}^P \sqrt{1 - \frac{x^2}{a_p^2} - \frac{y^2}{b_p^2}} \quad (15)$$

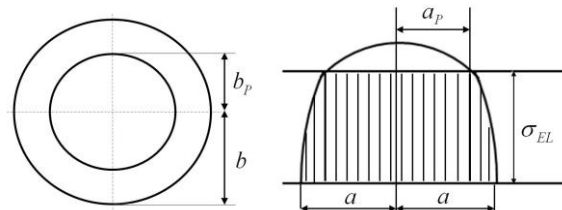


Figure 4. Contact stress distribution for elastic-plastic spheres.

### 2.3. Contact deformation and normal force

According to the Hertzian contact theory, the elastic contact deformation of the threaded interfaces of the PRSM can be expressed as [32]:

$$\sigma_E = \frac{2K(e)}{\pi m_a} \sqrt{\frac{9}{8} \left(\frac{1}{E'}\right)^2 F_n^2 \sum \rho} \quad (16)$$

Due to von Mises yield condition, the maximum contact pressure of the elastic limit can be written as

$$\sigma_{\max} = \frac{\sigma_S}{\sqrt{3k_{st}}} \quad (17)$$

where  $\sigma_s$  is the yield stress of the material and  $k_{st}$  is the constant of the value of 0.3 to 0.35.

Then, Eq. (16) can be expressed as

$$F_n = \frac{1}{3} \left( \frac{\pi m_a}{k(e)} \right)^{3/2} E' \left( \frac{1}{\sum \rho} \right)^{1/2} \delta_E^{3/2} \quad (18)$$

$$ab = \left( \frac{\pi m_a^2 m_b}{k(e)} \right) \left( \frac{1}{\sum \rho} \right) \delta_E \quad (19)$$

Substituting Eqs. (17), (18) and (19) into Eq. (13) yields the elastic limit stress and the corresponding normal force as follows:

$$\delta_{EL} = \frac{4}{3} \frac{k(e)}{\pi m_a} \left( \frac{\pi m_a m_b}{E'} \right)^2 \left( \frac{1}{\sum \rho} \right) \left( \frac{\sigma_s}{k} \right)^2 \quad (20)$$

$$F_{nL} = \frac{8}{9\sqrt{3}} \left( \frac{\pi m_a m_b \sigma_s}{k} \right)^3 \left( \frac{1}{E' \sum \rho} \right)^2 \quad (21)$$

If the stress-strain relationship of the elastoplastic material follows in the idealized elastic-plastic model, the normal force of the contact area is given as [33]

$$F_{n1} = F_{nL} + \frac{1}{2} k_P E' \delta_{EL}^{1/2} (\delta - \delta_{EL}) \quad (22)$$

where  $k_P$  is the modulus of the plastic contact strain as

$$k_P = \left( \frac{\pi m_a}{k(e)} \right)^{3/2} \left( \frac{1}{\sum \rho} \right)^{1/2} \quad (23)$$

The additional contact stress occurs at the contact interfaces during the plastic loading from the above assumptions.

$$\frac{2}{E'_P} = \frac{(1 - \mu_1^2)}{E_{P1}} + \frac{(1 - \mu_2^2)}{E_{P2}} \quad (24)$$

where  $E_{P1}$  and  $E_{P2}$  are the hardening modulus of two contact objects.

The additional normal force  $F_{nP}$  due to the hardening effect can be derived as

$$F_{nP} = \frac{1}{3} k_P E'_P (\delta - \delta_{EL})^{3/2} \quad (25)$$

So the additional maximum contact stress can be written as

$$\sigma_{\max}^P = \frac{3F_{nP}}{2\pi a_p b_p} \quad (26)$$

where  $a_p$  and  $b_p$  being the half lengths of the major and minor axis of the elliptical contact surface of the elastic limit.

According to the linear strain-hardening elastic-plastic model, the total normal force at the contact

interface is sum of the normal force  $F_{n1}$  due to idealized elastic-plastic model and the additional normal force  $F_{nP}$  due to the hardening effect.

$$F_n = F_{n1} + F_{nP} = F_{nL} + \frac{1}{2} k_P E' \delta_{EL}^{1/2} (\delta - \delta_{EL}) + \frac{1}{3} \left( \frac{\pi m_a}{k(e)} \right)^{3/2} E' \left( \frac{1}{\sum \rho} \right)^{1/2} \delta_E^{3/2} \quad (27)$$

### 3. Static load carrying capacity of PRSM.

#### 3.1. Simplified model of the static load distribution

Figure 5 shows the force analysis of PRSM in contact with a single mechanism of threads under the loads of axial force  $F_a$ , radial force  $F_r$ , tangential force  $F_t$  between the roller and screw.

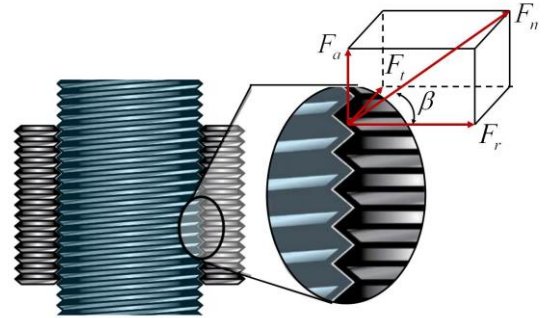


Figure 5. Diagram of screw and roller contact force.

The static load distribution across the thread turns can be obtained as follows:

$$\begin{cases} F_a(i) = F_n(i) \sin \beta \cos \lambda \\ F_n(i-1)^{3/2} = F_n(i)^{2/3} + \frac{Zp}{4(C_S + C_N)} \\ \left( \frac{1}{E_S A_S} + \frac{1}{E_N A_N} \right) \sin^2 \beta \cos^2 \lambda \sum_{j=i}^{\tau} F_n(j) \\ \sum_{i=1}^{\tau} F_a(i) = F \end{cases} \quad (28)$$

where  $\lambda$  is the helix angle of the roller thread,  $\tau$  refers to the number of roller thread turns,  $Z$  is the roller number,  $E_S$  is the equivalent Young's modulus of the screw and roller,  $E_N$  is the equivalent Young's modulus of the nut and roller,  $C_S$  is the screw rigidity,  $C_N$  is the nut rigidity,  $p$  is the pitch, and  $F$  is the axial load of the PRSM.

$A_S$  and  $A_N$  are the effective contact area of the screw and the nut, respectively, which can be derived as

$$A_S = \frac{\pi d_S^2}{4} \quad (29)$$

$$A_N = \frac{\pi(D_N^2 - d_N^2)}{4} \quad (30)$$

with  $D_N$  being the external diameter of the nut.

### 3.2. Static load carrying capacity

The roller screw mechanisms should be selected based on the basic static load carrying capacity  $C_{oa}$ , when they are subjected to continuous or intermittent shock loads, while stationary or rotating at very low speed for short duration.

The permissible load is determined by the permanent deformation caused by the load acting at the contact points.

The static load carrying capacity  $C_{oa}$  is, according to ISO standards, the purely axially and centrally applied static load which creates, by calculation, a total permanent deformation equal to 0.0001 of the diameter of curvature of the rolling element.

Considering the static load fluctuation across the thread turns to have a uniform distribution that the static load carrying capacity  $C_{oa}$  can be derived as

$$C_{oa} = (F_{nL} + \frac{1}{6} k_p \frac{d_R}{\cos \beta} \cdot 10^{-4} \cdot (3E' \delta_{EL}^{1/2} + 2E'_p \sqrt{\frac{d_R}{\cos \beta}} \cdot 10^{-2})) Z \tau_0 \sin \beta \cos \lambda \quad (31)$$

## 4. Analysis and discussion

### 4.1. Modelling of FE

In this paper, the structural parameters of the PRSM are taken in Table 1 as an example.

**Table 1**

**Structural parameters of the PRSM.**

Structural Parameters	Screw	Roller	Nut
Nominal radius $r$	15mm	5mm	25mm
Flank angle $\beta$	45°	45°	45°
Helix angle $\lambda$	6.057°	3.643°	3.643°
Number of starts $n$	5	1	5
Pitch $p$	2mm	2mm	2mm
Profile radius of roller thread $R$	/	7.071mm	/

According to the structural parameters of the PRSM listed in Table 1, the contact thread pairs at the screw/roller and roller/nut interfaces are developed, as shown in Figure 6.

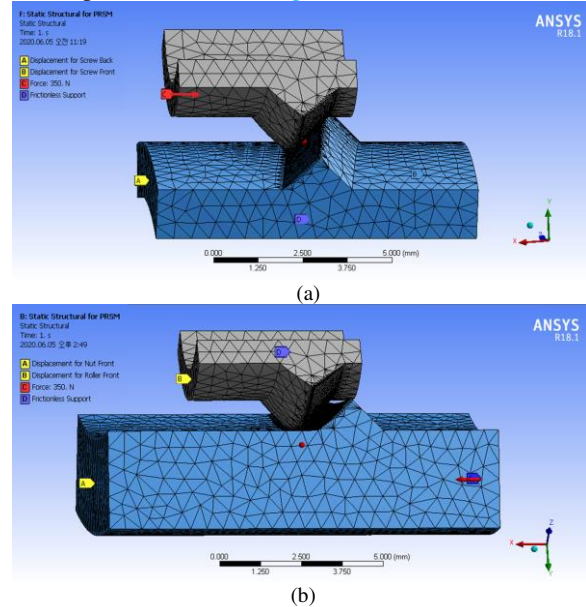


**Figure 6.** Contact model of (a) screw/roller interface and (b) roller/nut interface.

Meshing is based on the 4-node Tetrahedron non-coordinated solid element CPS4I, and the local contact area is densified.

The contact model of the screw thread and roller thread has 668,126 elements and 691,058 nodes. Similarly, the contact model of the roller thread and nut thread has 742,346 elements and 769,258 nodes.

In these numerical models, the material is GCr15, whose density is  $\rho=7810 \text{ kg/m}^3$ , elastic modulus is  $E=212\text{GPa}$ , and Poisson's ratio is  $\mu=0.29$ .

In the FE model, the axial loads and constraints are added to the PRSM model in the analysis to simulate the movements of the nut with only axial displacement, the roller with rotation and axial displacement, and the screw with only rotation displacement. The nut only has axial displacement degrees of freedom, and it has no degrees of freedom in other directions.

The lead screw has a rotational degree of freedom around its central axis.

The roller has rotational and axial displacement degrees of freedom and the axial concentrated force is defined on the left face of the nut.

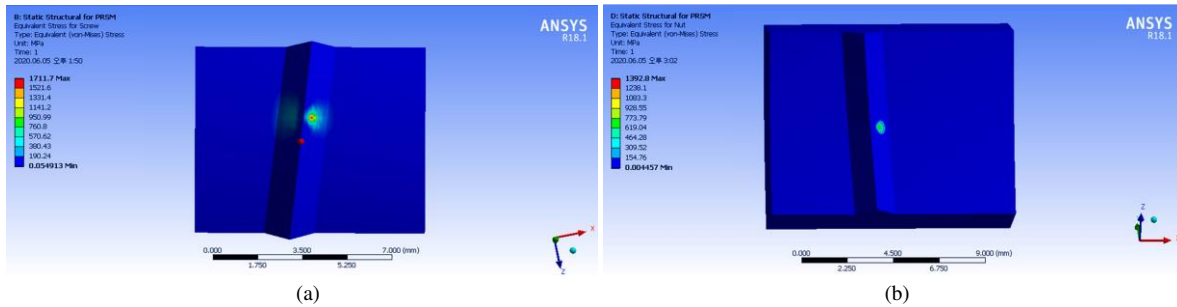


Figure 7. The von Mises stress distribution of (a) screw and (b) nut contact interface.

4.2. Contact stress and strain analysis of the PRSM.

When the axial force applied on the contact thread pairs is 350N, the von Mises stress distribution across the thread turns is shown in Figure 7.

From the simplified model of the static load distribution, the maximum value of contact normal force at the screw/roller and roller/nut interfaces is about 495.977N.

As shown in Figure 7, the maximum value of von Mises stress at the screw interface is 1711.7MPa and the maximum value of von Mises stress at the nut interface is 1392.8MPa.

Therefore, the maximum von Mises stress at the screw/roller interface is bigger than the roller/nut interface with the same axial load.

And the FE calculation results of contact deformation at the screw/roller and roller/nut interfaces are as shown in Figures 8 and 9.

As shown in Figures 8 and 9, the maximum elastic contact strain at the screw/roller interface of the PRSM is  $5.4355 \times 10^{-3}$  mm/mm and the maximum elastic contact strain at the roller/nut interface is  $5.0937 \times 10^{-3}$  mm/mm.

At this time, the plastic strain occurs at screw/roller interface but the plastic strain doesn't occur at roller/nut interface because its maximum stress value is less than the yield stress of 1700MPa.

As shown in Figure 8(b), the maximum contact equivalent plastic strain at the screw/roller interface is  $6.2277 \times 10^{-4}$  mm/mm.

According to Hooke's law, the total plastic deformation at the screw/roller interface is  $12.4454 \times 10^{-4}$  mm, which is less than 0.0001 of the diameter of curvature of the rolling element 14.1422mm. This means that the designed PRSM meets the requirements for the rated static load carrying capacity. And then the total contact strain can be calculated as sum of the elastic and plastic strain at the thread interface with the axial load.

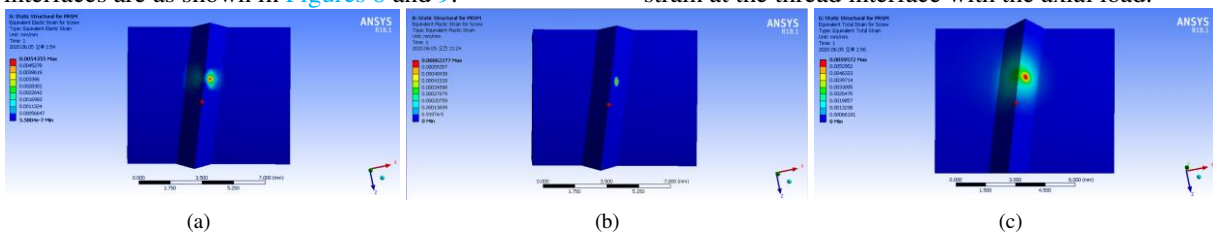


Figure 8. Diagram of (a) elastic and (b) plastic and (c) total contact strain of screw.

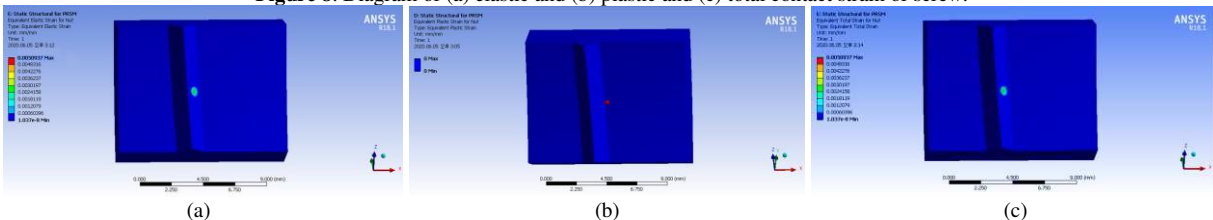


Figure 9. Diagram of (a) elastic and (b) plastic and (c) total contact strain of nut.

The total contact strain at screw/roller interface is  $5.9572 \times 10^{-4}$  mm/mm and the total contact strain at roller/nut interface is  $5.0937 \times 10^{-3}$  mm/mm.

The FE calculation results about the contact characteristics of the designed PRSM are consistent with analytical results.

The results also show that the equivalent finite element model of the PRSM proposed in this paper is reasonable.

### 4.3. Comparison of the calculation results.

#### 4.3.1 Static load carrying capacity of the different PRSM.

The static load carrying capacity of the PRSM can be obtained by substituting the screw mechanism parameters depending on the various elastic-plastic models (EPMs) of its material.

The calculation results about static load carrying capacity of the different roller screw mechanisms, which have a screw pitch of 1mm, five-starts thread of screw and nut, 10 rollers, are listed in Table 2.

**Table 2**  
**Static load carrying capacity of the different PRSM.**

PRSM type	Static load carrying capacity <i>Coa, kN</i>	
	Idealized EPM	Linear strain-hardening EPM
<i>SRC 15 × 5</i>	31.604	31.672
<i>SRC 21 × 5</i>	65.565	65.705
<i>SRC 30 × 5</i>	158.686	159.026
<i>SRC 39 × 5</i>	250.444	250.98
<i>SRC 48 × 5</i>	451.759	452.727

As shown in Table 2, the calculation results about the static load carrying capacity of PRSM depending on various EPMs increase with increasing nominal diameter of the screw.

And the linear strain-hardening EPM is bigger than the idealized EPM.

**Table 3**

**Contact characteristics of the PRSM.**

Contact normal force (N)	Screw/roller interface			Nut/roller interface		
	Von Mises stress(MPa)	Elastic contact deformation(mm)	Plastic contact deformation(mm)	Von Mises stress(MPa)	Elastic contact deformation(mm)	Plastic contact deformation(mm)
200	1334.7	0.0063	-	1104.3	0.0055	-
400	1681.6	0.0100	-	1319.4	0.0087	-
600	1714.1	0.0102	0.0031	1592.7	0.0114	-
800	1741.9	0.0102	0.0064	1714.2	0.0130	0.0008
1000	1788.3	0.0102	0.0096	1738.2	0.0130	0.0032

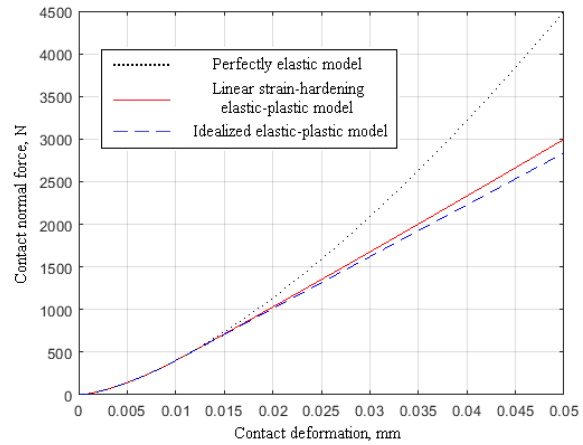


**Figure 10.** The relationship between the contact normal force and contact deformation due to different EPMs.

#### 4.3.2 Contact stress and deformation of the PRSM.

Figure 10 shows the relationship between normal force and contact deformation at the screw/roller interface of the typed “SRC 30×10” PRSM depending on various EPMs of the material.

As can be seen from Figure 10, the plastic component of the linear strain-hardening elastic-plastic loading curve is a straight line tangent to the elastic one in its point of intersection and the linear strain-hardening elastic-plastic loading curve is over the idealized elastic-plastic loading curve.

The analytical solutions about the contact stress and deformation at the screw/roller interfaces of the PRSM due to linear strain-hardening EPM are shown in Table 3.

At this time, the contact normal force corresponding to critical elastic deformation is 413.3N at the screw/roller interface and 729.57N at the roller/nut interface.

The maximum von Mises stress at the contact thread interface increases with the increase of the contact normal force as shown in Table 3.

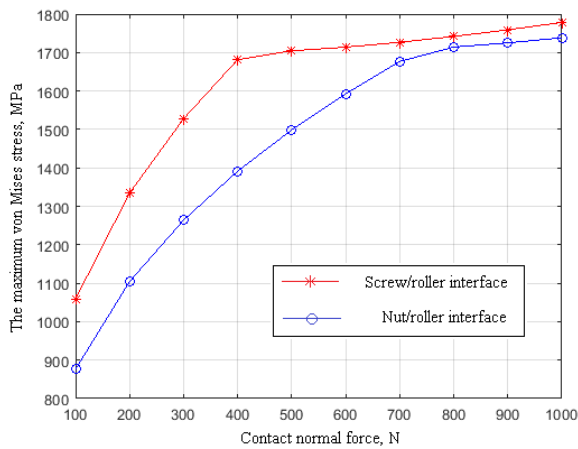


Figure 11. The maximum von Mises stress at the contact thread interface of a PRSM.

When the von Mises stress in the contact area has reached the yield stress of the material of a PRSM, the elastic deformation doesn't occur anymore and the plastic deformation begins to occur as the external load increases. The von Mises stress at the screw/roller and nut/roller contact interface can be changed with the variation of the contact normal force as shown in Figure 11.

Besides, it can be also seen from Figure 11 that the contact stress at the screw/roller interface is bigger than the roller/nut interface.

Hence, the contact characteristics of screw/roller interfaces are mainly considered in the static design calculation of a PRSM and the total contact deformation is obtained by summing the elastic and plastic deformation.

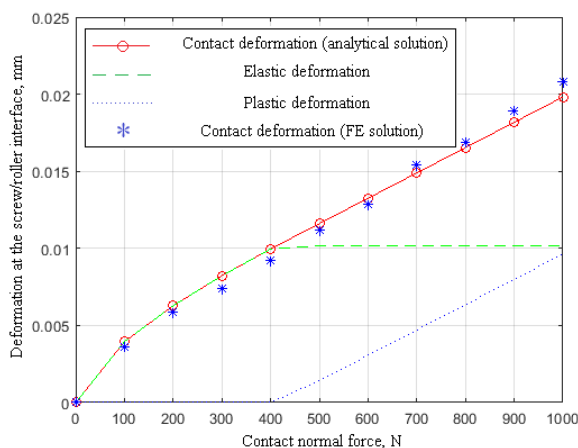


Figure 12. Contact deformation at the screw/roller interface with different contact normal force

The diagram of the comparison between the analytical solution and numerical solution of FE about contact deformation with the variation of the contact normal force at the screw/roller interface is shown in Figure 12.

Figure 12 shows that the relative error between the two result sets is less than or equal to 5%, and the range of the error is acceptable.

Therefore, the analytical model proposed in this paper can be used to study the parametric sensitivity of the design.

### 5. Conclusions

- (1) The static contact stress and strain in the contact area are very important for studying the wear, transmission accuracy and efficiency of a PRSM. So the contact analysis is performed due to linear strain-hardening elastic-plastic model and the analytical model presented in this paper is verified by the comparison of the results between the theory model and FE model.
- (2) The static load carrying capacity of a PRSM is calculated based on the simplified model of static load distribution among screw, rollers and nut. The results show that the contact stress at the roller/nut interface is far less than that of the screw side and the contact stress and strain at the screw/roller interface are the main contact characteristics in the static design calculation of a PRSM.
- (3) The relative error between the analytical solution and numerical solution of FE about contact characteristics at the screw/roller interfaces are less than or equal to 5%, and the range of the error is acceptable.

### Author's Contributions

NS-KIM was in charge of the whole trial; KH-KIM, and SH-JONG wrote the manuscript; KH-KIM assisted with sampling and laboratory analyses. All authors read and approved the final manuscript.

### Competing interests

The authors declare no competing financial interests.

### Author's information

Nam Su Kim, born in 1986, is currently a professor at *Faculty of Mechanics, Kim Il Sung University, Korea*. His research interests include theory of mechanism and machinery dynamics. E-mail: [NS.KIM@star-co.net.kp](mailto:NS.KIM@star-co.net.kp)

Kyong Ho Kim, born in 1963, is currently a PhD candidate at *Faculty of Mechanics, Kim Il Sung University, Korea*. His research interests include contact mechanics. E-mail: [KH.KIM@star-co.net.kp](mailto:KH.KIM@star-co.net.kp).

Sin Hyok Jong, born in 1996, is currently graduate student at *Faculty of Mechanics, Kim Il Sung University, Korea*. His research interests include contact mechanics. E-mail: [SH.JONG@star-co.net.kp](mailto:SH.JONG@star-co.net.kp).

### Funding

The authors disclosed receipt of the following financial support for the research, authorship, and/or publication of this article: This paper was supported by National Science and Technology Major Project (2016ZX04004007).

### References

- [1] Rollvis Swiss, Satellite roller screws, *catalogue* 2019.
- [2] S. Sandu, N. Biboulet, D. Nelias, F. Abevi, An efficient method for analyzing the roller screw thread geometry, *Mech. Mach. Theory* 126 (2018) 243–264.
- [3] S. Ma, G. Liu, R. Tong, X. Zhang, A new study on the parameter relationships of planetary roller screws, *Math. Probl. Eng.* 2012 (2012) 1–29. Article ID 340437.
- [4] P.A. Sokolov, O.A. Ryakhovskiy, D.S. Blinov, A. Laptev, Kinematics of planetary roller-screw mechanisms, *Vestn. MGTU Mashinostr* 2005 (2005) 3–14 in Russian.
- [5] M.H. Jones, S.A. Velinsky, Kinematics of roller migration in the planetary roller screw mechanism, *J. Mech. Des.* 134 (6) (2012) 061006–061006-6
- [6] S.A. Velinsky, B. Chu, T.A. Lasky, Kinematics and efficiency analysis of the planetary roller screw mechanism, *ASME J. Mech. Des.* 131 (1) (2009) 011016.
- [7] A.V. Zhdanova, V.V. Morozova, Theoretical study of the load distribution on the threads for roller screw mechanisms of a friction type, in: *International Conference on Industrial Engineering, ICIE 2016, Procedia Engineering*, 150, 2016, pp. 992–999.
- [8] J. Rys, F. Lisowski, The computational model of the load distribution between elements in a planetary roller screw, *J. Theor. Appl. Mech.* 52 (3) (2014) 699–705.
- [9] Zhang, G. Liu, R. Tong, S. Ma, Load distribution of planetary roller screw mechanism and its improvement approach, proceedings of the institution of mechanical engineers, Part C: *J. Mech. Eng. Sci.* 230 (18) (2016) 3304–3318.
- [10] M.H. Jones, S.A. Velinsky, Stiffness of the roller screw mechanism by the direct method, *Mech. Based Des. Struct. Mach.* 42 (1) (2014) 17–34.
- [11] F. Abevi, A. Daidie, M. Chaussumier, M. Sartor, Static load distribution and axial stiffness in a planetary roller screw mechanism, *J. Mech. Des.* 138 (1) (2016) 012301–012308.
- [12] F. Abevi, A. Daidie, M. Chaussumier, S. Orioux, Static analysis of an inverted planetary roller screw mechanism, *J. Mech. Rob.* 8 (4) (2016) 041020–041020-14.
- [13] K. Li, P.Q. Ye, X.Y. Zhou, Q. Xu, Transmission characteristics of precise planetary roller screw, *Opt. Precis. Eng.* 24 (8) (2016) 1908–1916.
- [14] S.J. Ma, W. Cai, L.P. Wu, G. Liu, C. Peng, Modelling of transmission accuracy of a planetary roller screw mechanism considering errors and elastic deformations, *Mech. Mach. Theory* 134 (2019) 151–168.
- [15] M.I. Mamaev, V.V. Morozov, O.V. Fedotov, V.N. Filimonov, Precision of a roller screw actuator transmission for a radio telescope, *Russ. Eng. Res.* 35 (12) (2015) 919–923.
- [16] G. Auregan, V. Fridrici, P. Kapsa, F. Rodrigues, Experimental simulation of rolling-sliding contact for application to planetary roller screw mechanism, *Wear* 332–333 (2015) 1176–1184.
- [17] G. Auregan, V. Fridrici, P. Kapsa, F. Rodrigues, Wear behavior of martensitic stainless steel in rolling-sliding contact for planetary roller screw mechanism: study of the WC/C solution, *Tribol. Online* 11 (2) (2016) 209–217.
- [18] D.W. Zhang, S.D. Zhao, S.B. Wu, Q. Zhang, S.Q. Fan, J.X. Li, Phase characteristic between dies before rolling for thread and spline synchronous rolling process, *Int. J. Adv. Manuf. Technol.* 81 (1–4) (2015) 513–528.
- [19] X.J. Fu, G. Liu, R.T. Tong, S.J. Ma, Teik C. Lim, A nonlinear six degrees of freedom dynamic model of planetary roller screw mechanism, *Mech. Mach. Theory* 119 (2018) 22–36.
- [20] M.H. Jones, S.A. Velinsky, T.A. Lasky, Dynamics of the planetary roller screw mechanism, *J. Mech. Rob.* 8 (1) (2016) 014503–014506.
- [21] G. Qiao, G. Liu, S.J. Ma, Y.W. Wang, P. Li, Teik C. Lim, Thermal characteristics analysis and experimental study of the planetary roller screw mechanism, *Appl. Therm. Eng.* 149 (2019) 1345–1358.
- [22] D.S. Blinov, O.A. Ryakhovskiy, P.A. Sokolov, Numerical method of determining the point of initial thread contact of two screws with parallel axes and different thread inclinations, *Vestn. MGTU Mashinostr.* 3 (1996) 93–97.
- [23] M.H. Jones, S.A. Velinsky, Contact kinematics in the planetary roller screw mechanism, *J. Mech. Des.* 135 (5) (2013) 051003–051010.
- [24] Y.Q. Liu, J.S. Wang, H.G. Cheng, Y.P. Sun, Kinematics analysis of the roller screw based on the accuracy of meshing point calculation, *Math. Probl. Eng.* 2015 (2015) 1–10.
- [25] O.A. Ryakhovskiy, F.D. Sorokin, A.S. Marokhin, Calculation of radial displacements of nut and rollers axes and the position of a contact between the nut and the roller thread in an inverted planetary roller screw mechanism, *Higher Educ. Inst. Mach. Build.* 11 (2013) 12–19.

- [26] X.J. Fu, G. Liu, S.J. Ma, R.T. Tong, A comprehensive contact analysis of planetary roller screw mechanism, *J. Mech. Des.* 139 (1) (2017) 012302–012311.
- [27] S. Sandu, N. Biboulet, D. Nelias, F. Abevi, Analytical prediction of the geometry of contact ellipses and kinematics in a roller screw versus experimental results, *Mech. Mach. Theory* 131 (2019) 115-136.
- [28] S. Ma, L. Wu, X. Fu, Y. Li, G. Liu, Modelling of static contact with friction of threaded surfaces in a planetary roller screw mechanism, *Mech. Mach. Theory* 139 (2019) 212-236.
- [29] M. Yousef Hojjat, A. Mahdi, A comprehensive study on capabilities and limitations of roller-screw with emphasis on slip tendency, *Mech. Mach. Theory* 44 (10) (2009) 1887–1899.
- [30] L. Zu, Z. Zhang, and L. Gao, Design and bearing characteristics of planetary roller screws based on aerospace high-load conditions, *Advances in Mechanical Engineering* 2018, Vol. 10(11)
- [31] J.F. Antoine, C. Visa, C. Sauvey, G. Abba, Approximate analytical model for hertzian elliptical contact problems, *ASME J. Tribol.* 128 (2006) 660-663.
- [32] K. Johnson, Contact Mechanics, 9th ed., *Cambridge University Press*, 1985.
- [33] T.A. Harris, M.N. Kotzalas, Rolling Bearing Analysis, 5th ed., *Taylor and Francis*, 2007.

# Figures

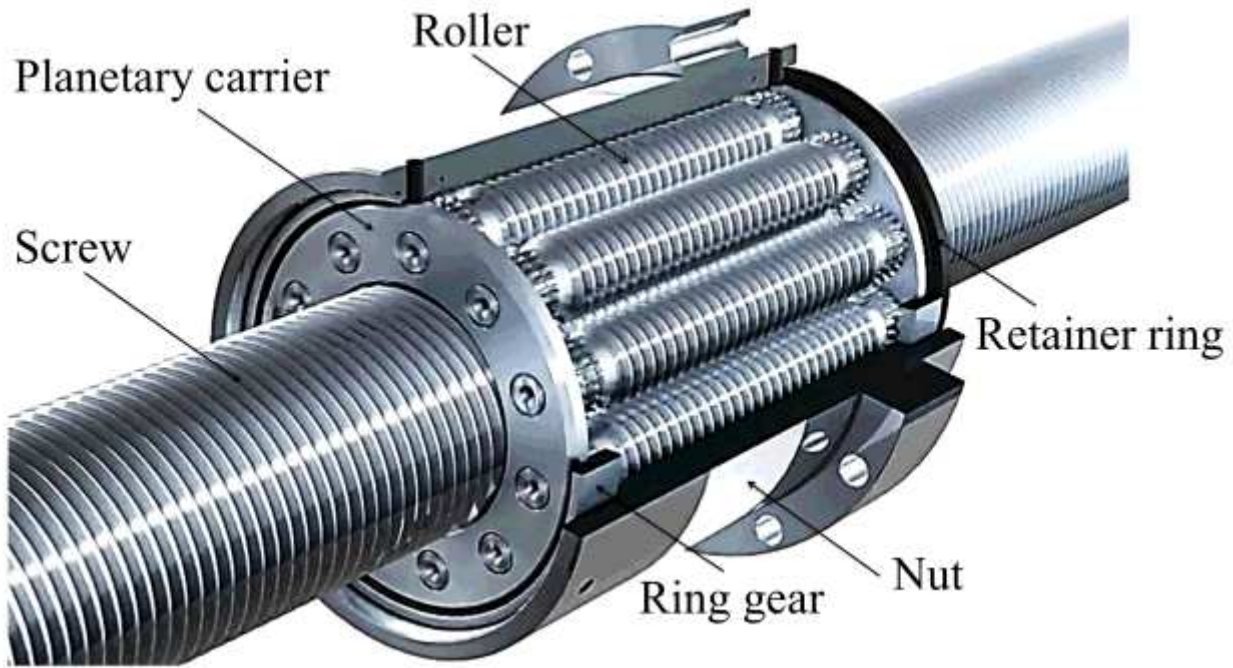


Figure 1

Structure of the PRSM.

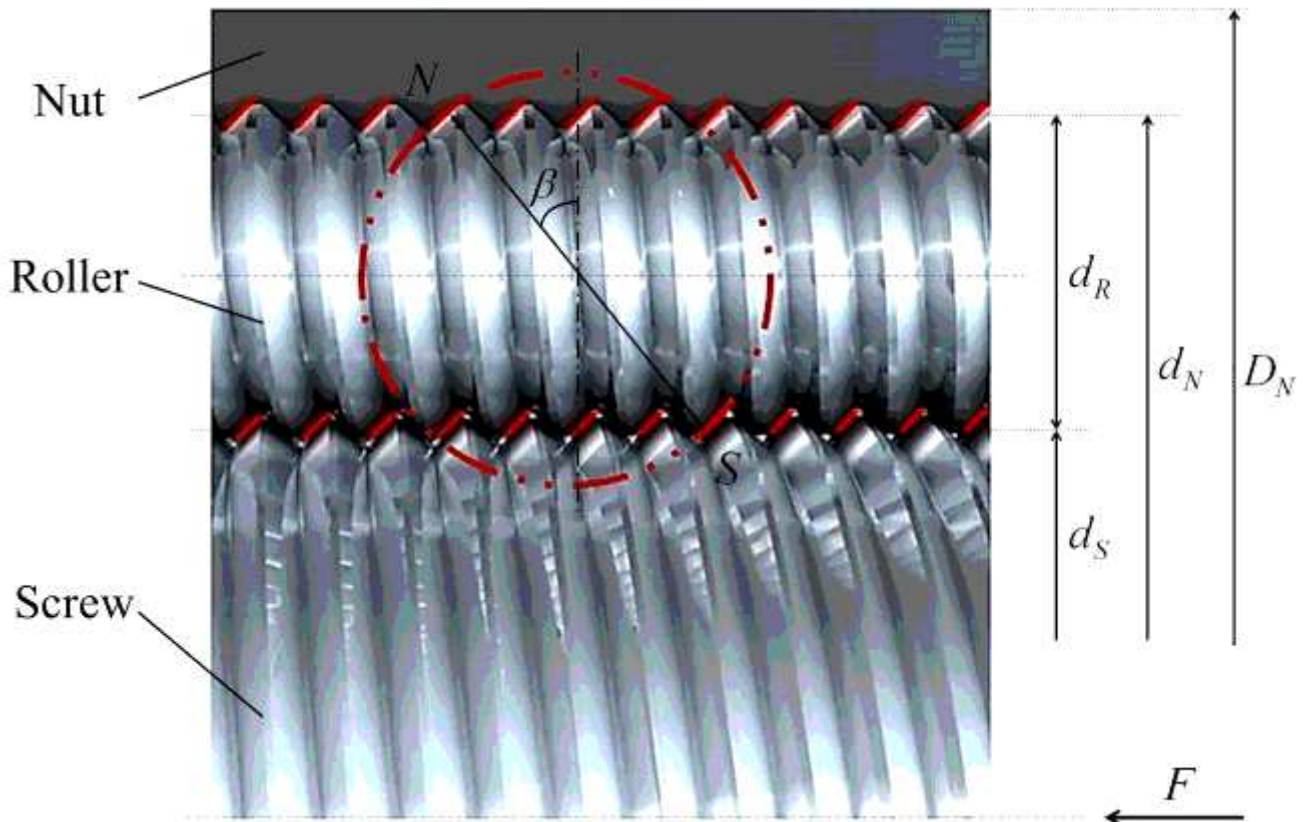


Figure 2

Structure of the PRSM.

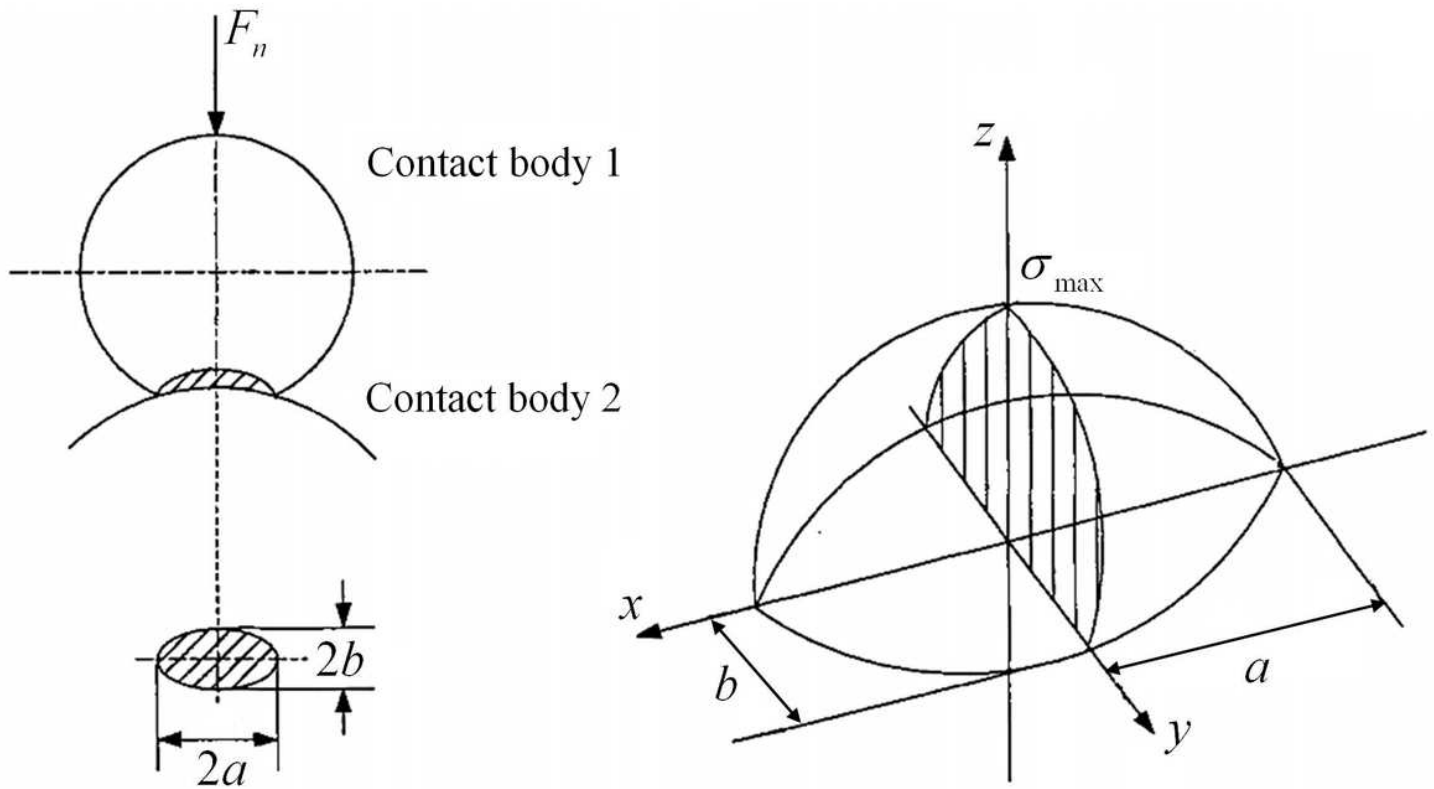


Figure 3

Elastic contact stress over the ellipse contact area.

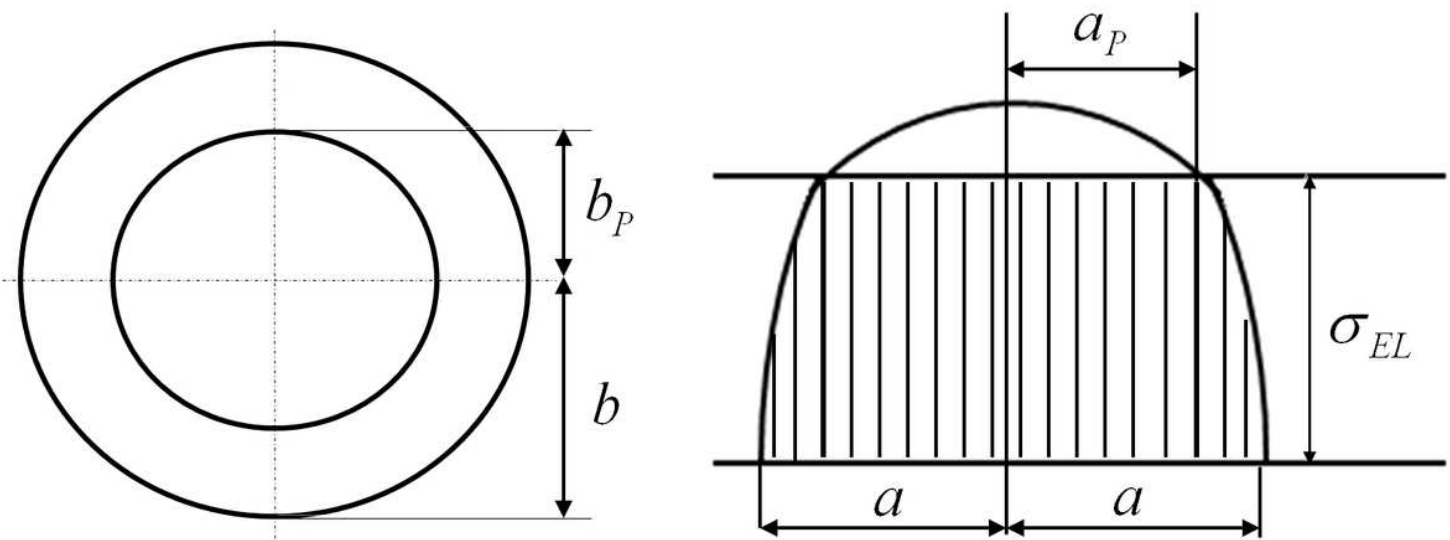


Figure 4

Contact stress distribution for elastic-plastic spheres.

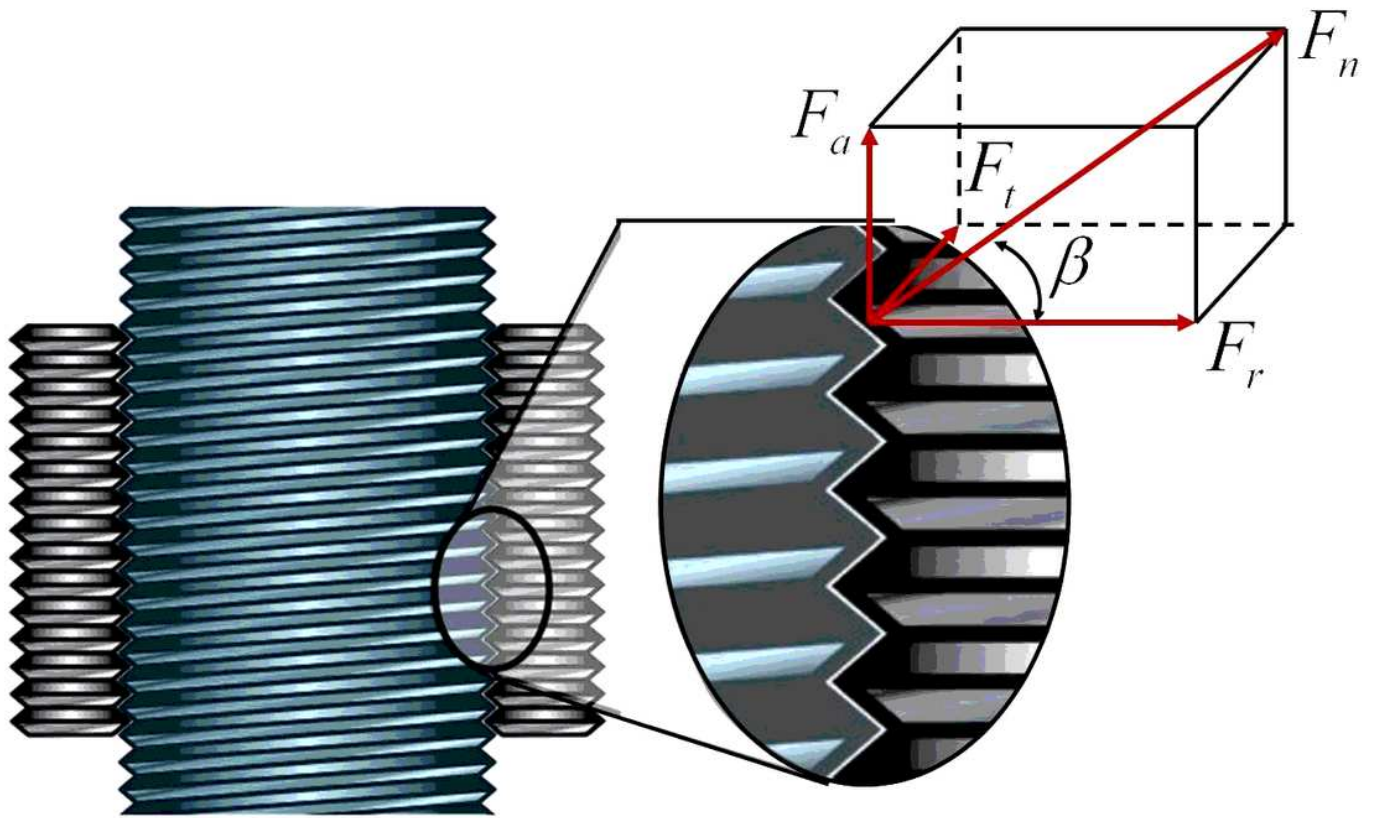
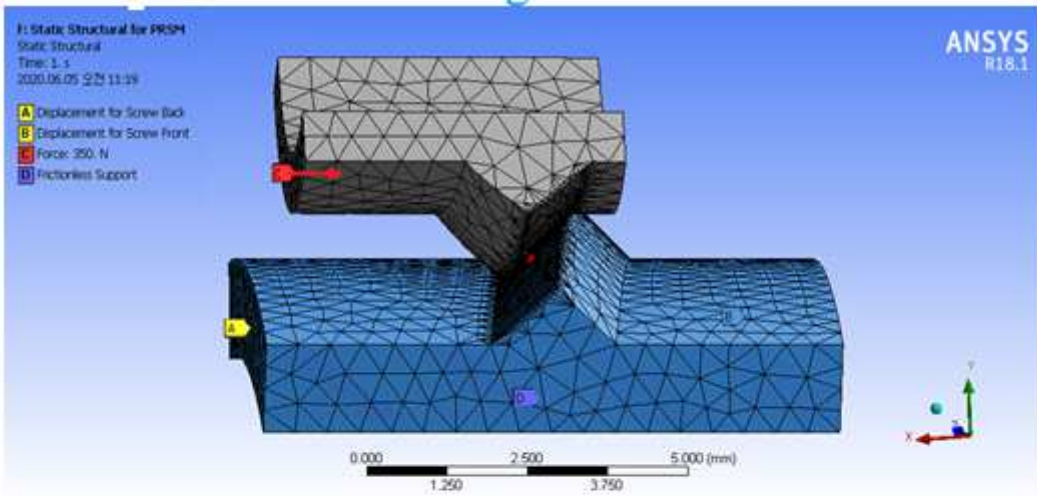
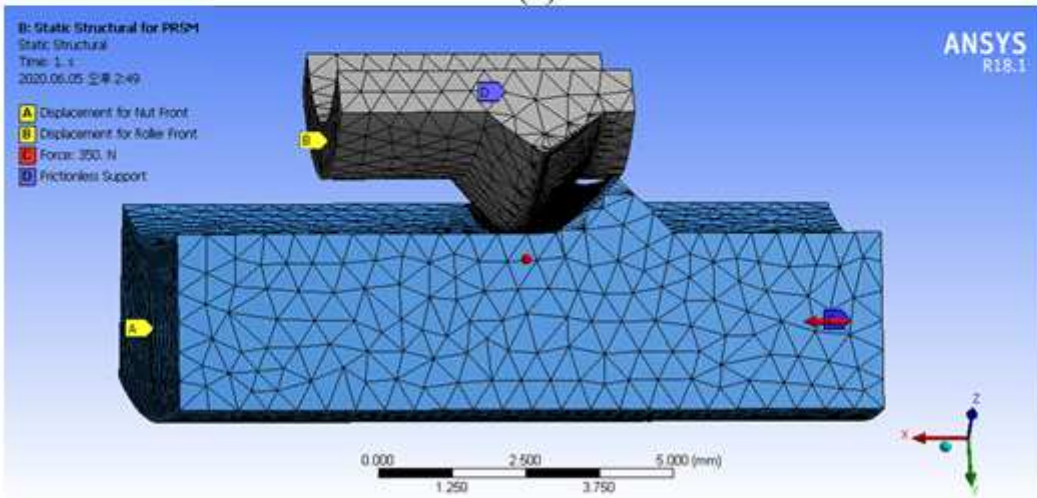


Figure 5

Diagram of screw and roller contact force.



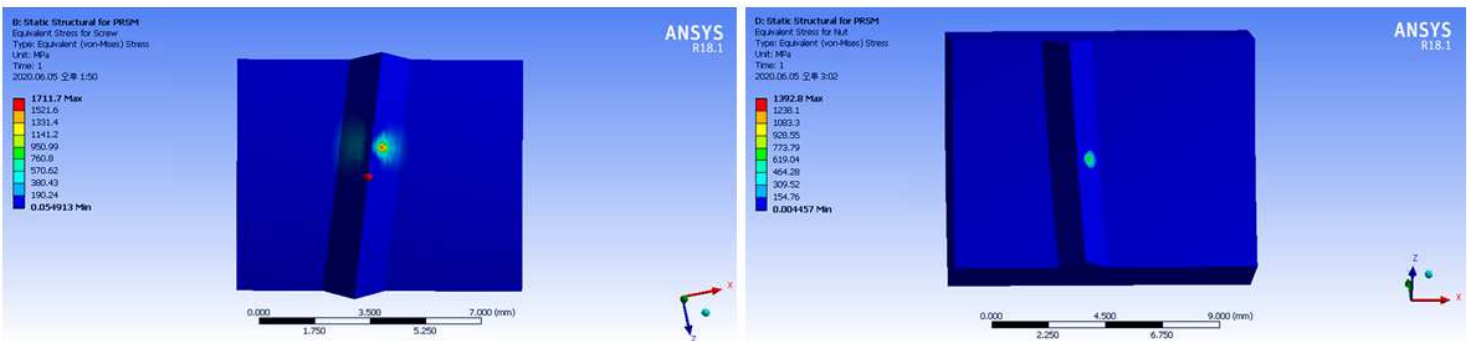
(a)



(b)

Figure 6

Contact model of (a) screw/roller interface and (b) roller/nut interface.



(a)

(b)

Figure 7

The von Mises stress distribution of (a) screw and (b) nut contact interface.

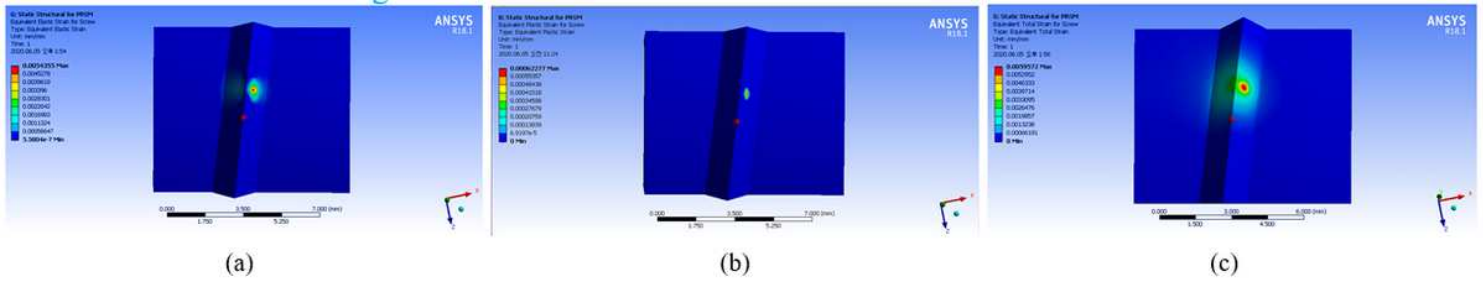


Figure 8

Diagram of (a) elastic and (b) plastic and (c) total contact strain of screw.

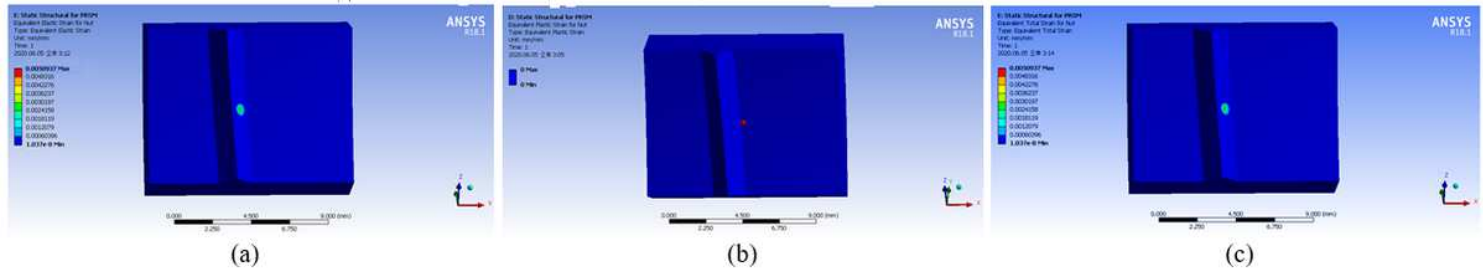


Figure 9

Diagram of (a) elastic and (b) plastic and (c) total contact strain of nut.

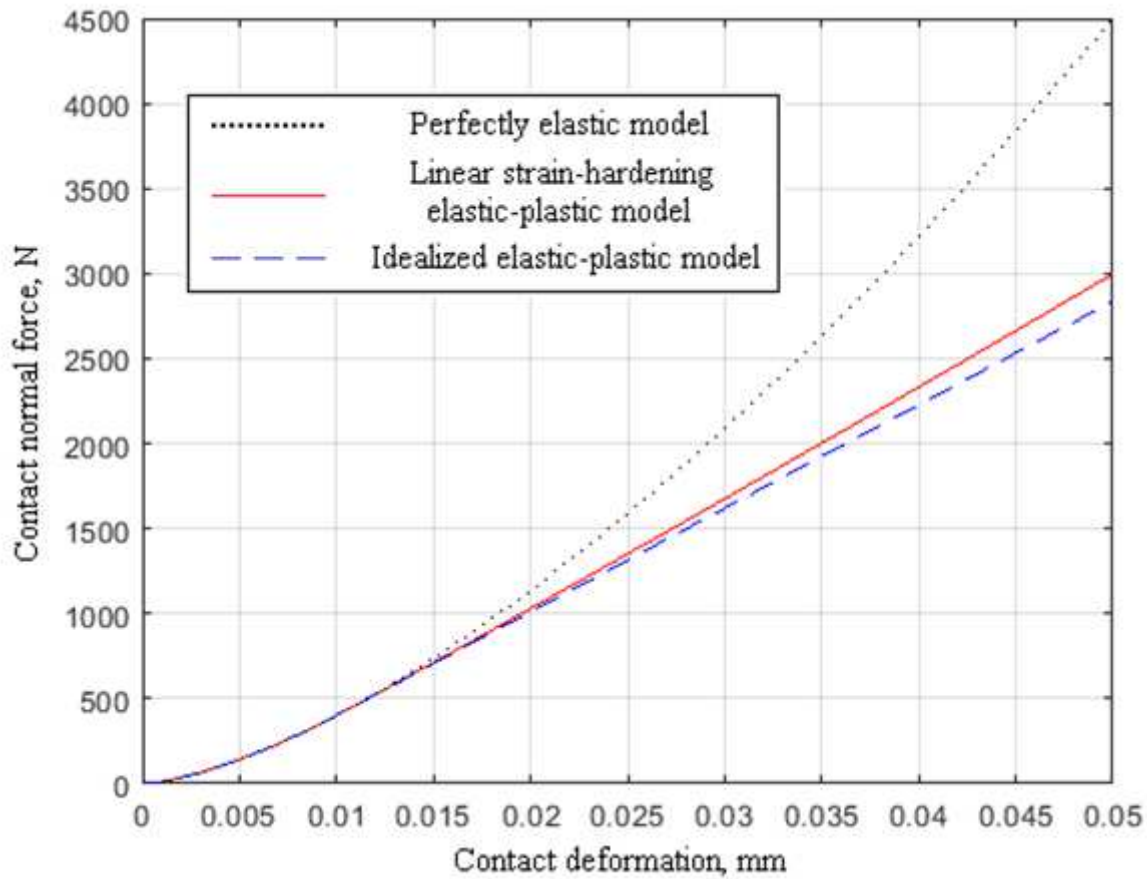


Figure 10

The relationship between the contact normal force and contact deformation due to different EPMs.

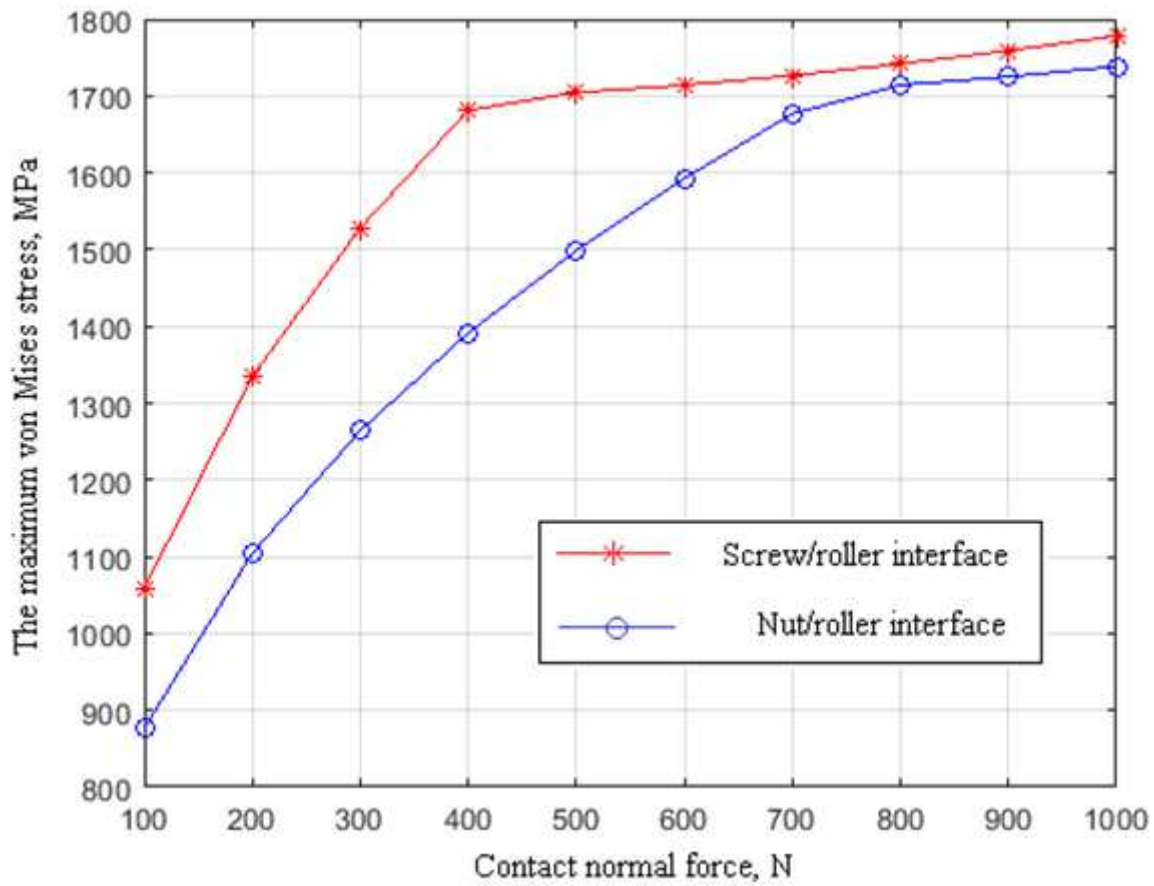


Figure 11

The maximum von Mises stress at the contact thread interface of a PRSM.

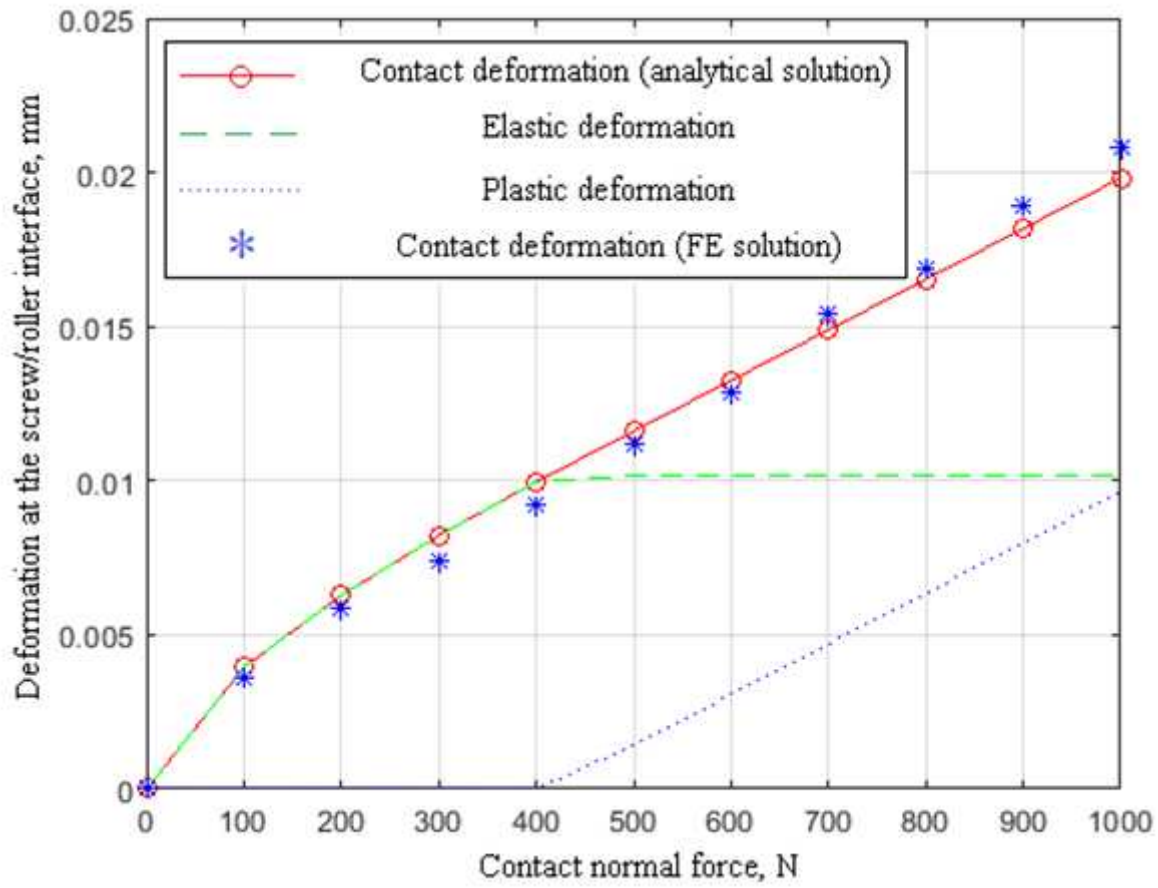


Figure 12

Contact deformation at the screw/roller interface with different contact normal force